

SEVERE HAIL DETECTION: AN ADAPTIVE ALGORITHM FOR ANOMALOUS ATTENUATION CORRECTION AND NEW INSIGHTS FROM SCATTERING SIMULATIONS AT C-BAND

Matthias B. Schmidt^{1,*}, Silke Trömel¹, Alexander V. Ryzhkov², Clemens Simmer¹

¹University of Bonn, Bonn, Germany

²CIMMS/Univ. of Oklahoma, Norman, Oklahoma

1. INTRODUCTION

Large hail is a frequently occurring and sometimes devastating phenomenon, especially during summertime convective events. Many occasions of hail stones with diameters above 5 cm up to 14 cm have been reported and confirmed in the last years in central Europe.

Concepts and algorithms to detect and distinguish large hail from small hail or rain with polarimetric radars at S band have been discussed and published in the literature (e.g. Ryzhkov *et al.*, 2013b, Ortega *et al.*, 2016). Similar algorithm has to be developed for utilization at C-band radars on operational weather radar networks in Europe, including Germany.

While the strong attenuation at C band allows for the identification of hail mixed with rain and for the discrimination between different hail sizes, it also hampers quantitative precipitation estimation. Anomalously high attenuation due to large, wet hail may occur, which makes the use of signals beyond hail-affected range bins challenging. Therefore, a reliable correction of anomalous attenuation is mandatory.

Testud *et al.* (2000) introduced the ZPHI method to correct for attenuation in rain using the total span of differential phase Φ_{DP} as a constraint. Ryzhkov *et al.* (2013b) presented a modified ZPHI method, which is capable of correcting attenuation in hail at S band but requires certain assumptions regarding the distribution of hydrometeor types along the radial in the shadow of hail.

2. DATA

We use the German polarimetric radar network of the German Weather Service (DWD) covering an area

of more than 357000 km² as primary radar data source. For evaluation, observations of hail occurrence and size are taken from the national disdrometer network and the growing European Severe Weather Database (ESWD). Figure 1 shows the coverage of the available national radar network and disdrometer stations.

3. APPLIED ALGORITHMS

Different algorithms or modifications of algorithms for hail attenuation correction have been developed and tested. We will present here algorithms to be used for hail attenuation correction at C band. A severe hailstorm occurring on 23th June 2016 over the Brabant/Netherlands and North Rhine-Westphalia/Germany, will serve as an example event to illustrate the performance of the algorithms.

3.1 Hotspot/ZPHI-method for C band

Ryzhkov *et al.* (2013b) introduces a hail attenuation correction based on the ZPHI-method. To use the ZPHI-method for hail, the propagation path through a hail bearing cell is separated into three segments assuming, that hail exists between the range (r_1, r_2), between rain intervals closer to the radar (r_0, r_1) and at the rear side of the hail core (r_2, r_m) as defined in Ryzhkov *et al.* (2013b). The three segments are chosen according to a certain reflectivity threshold (e.g., 50 dBZ), so that the reflectivity factor in the interval (r_1, r_2) is at or above the threshold.

The specific attenuation in hail A_h or rain is determined as (Testud *et al.*, 2000; Ryzhkov *et al.*, 2013b)

* *Corresponding author address:* Matthias B. Schmidt, University of Bonn, Meteorologisches Institut, Auf dem Hügel 13, 53121 Bonn, Germany; e-mail: MatthiasBSchmidt@uni-bonn.de.

$$A_h(r) = \frac{[Z_a(r)]^b (\exp[0.23b \cdot PIA(r_1, r_2)] - 1)}{I(r_1, r_2) + (\exp[0.23b \cdot PIA(r_1, r_2)] - 1) \cdot I(r, r_2)}, \text{ where} \quad (1)$$

$$I(r_1, r_2) = 0.46b \int_{r_1}^{r_2} [Z_a(s)]^b ds \text{ and} \quad (2)$$

$$I(r, r_2) = 0.46b \int_r^{r_2} [Z_a(s)]^b ds, \quad (3)$$

where Z_a is attenuated reflectivity factor expressed in linear scale and PIA is the two-way path-integrated attenuation.

It is assumed that A and Z are related according to a power-law ($A=aZ^b$), with the parameters a and b different in hail and rain. In our study we take the values of a and b from theoretical simulations presented in Table 1 in Ryzhkov *et al.* (2013b).

PIA in rain segments is estimated using differential phase Φ_{DP} as

$$PIA = \alpha_{rain} \Delta\Phi_{DP}, \quad (4)$$

where α_{rain} is the ratio of the specific attenuation A and the specific differential phase K_{DP} and $\Delta\Phi_{DP}$ is the total span of differential phase in the chosen rain segment. We assume α_{rain} is constant. A similar relation for PIA for hail, but with the α_{hail} determined as

$$\alpha_{hail} = \frac{\Delta Z}{\Delta\Phi_{DP,hail}} = \frac{\left(\frac{A_h(r_2)}{a}\right)^{\frac{1}{b}} - Z_a(r_2)}{\Phi_{DP}(r_2) - \Phi_{DP}(r_1)}, \quad (5)$$

where $A_h(r_2)$ is determined from equation (1) for rain at range r_2 .

Using the now estimated α_{hail} , equation (4) can be modified for use in hail (using α_{hail} and $\Delta\Phi_{DP,hail}$) to obtain PIA in hail. With this and equation (1) the specific attenuation in hail can be estimated.

$$\delta(r_2) - \delta(r_1) = \Phi_{DP}(r_2) - \Phi_{DP}(r_1) - \frac{1}{0.23b_h\alpha_h} \ln \left[1 + A_h(r_2) \cdot \frac{I(r_1, r_2)}{Z'(r_2 - 1)^{b_h} - A_h(r_2) \cdot I(r_2 - 1, r_2)} \right] \quad (8)$$

The full derivation of the equation (8) is in APPENDIX.

With the modifications to the Hotspot/ZPHI-method applied, realistic hail attenuation correction at C band can be done. For an event with up to 9cm hail diameter reported, this is shown in Figure 3. The corrected reflectivity factor indeed shows now the full extent of the major hail-bearing cell, but also a minor cell is now visible. However, such a correction is not applicable for all azimuths; these are shown in gray. Also, azimuths, where the signal was completely lost, cannot be recovered either.

As a byproduct of the algorithm, the α_{hail} value can be used as a rough hail size discrimination. As shown in Ryzhkov *et al.* (2013b), α_{hail} varies with hail size. Using the α_{hail} values, which were calculated to correct

With the attenuation known for all segments, the intrinsic reflectivity factor Z can be calculated as

$$Z(r) = Z_a(r) + 2 \int_0^r A_h(s) ds. \quad (6)$$

Following these equations an attenuation-correction method shows reasonable performance for selected cases at S band, where backscatter differential phase is smaller than at C band (Ryzhkov *et al.*, 2013b). Indeed, at C band, backscattering phase shift due to hail can be a problem and lead to anomalous specific attenuation calculations when applying the Hotspot/ZPHI-method. This shows up in Figure 2, where specific attenuation A is shown along one selected azimuth in blue. Discontinuities in A between the first two segments are clearly visible. This points to a need to take into account the backscatter differential phase for any ZPHI-based method at C band.

The discontinuities shown in Figure 2 before, are a most likely the result of neglected δ in equation (4), which has to be modified to include δ :

$$PIA(r_1, r_2) = \alpha[\Phi_{DP}(r_2) - \Phi_{DP}(r_1) - \alpha[\delta(r_2) - \delta(r_1)]]. \quad (7)$$

In order to estimate δ , equations will be inverted and continuity between the segments is demanded ($A_h(r_1) \rightarrow A_h(r_1+1)$ and $A_h(r_2) \rightarrow A_h(r_2+1)$). Estimated difference in δ is then

hail attenuation, a possible hail size category can be determined.

Comparison with ground reports is shown in Figure 4, where the estimated α_{hail} values for the same event are shown along with typical α_{hail} values for certain hail diameters. Additionally, an overview of all reports for that day and the range of reported maximum diameters from the ESWD is shown.

3.2 Multi-Interval ZPHI-method

The suggested modification of a Hotspot/ZPHI-method works fine, but lacks radial resolution for α_{hail} estimations. To increase the resolution, the scheme of three segments (rain, hail, rain in the shadow of hail) is replaced by a scheme with an arbitrary number of segments (similar to Le Bouar *et al.*, 2001). The

segments are no longer required to contain strictly rain or hail in a special order or number, except for the very last segment, which is still assumed to contain pure rain.

Multiple approaches to optimize the choice of selected segments have been tested. Segments were chosen by either fixed lengths, local Z minima or local Φ_{DP} minima. None of them worked outstanding, but local Φ_{DP} minima worked better than other approaches. Figure 5 shows a result of hail attenuation correction for the event on June 2016. However, overestimation of α_{hail} and Z is possible here.

3.3 Adaptive α -scheme

Using the standard ZPHI-method, as described in Testud *et al.* (2000), specific attenuation can be calculated for a certain, assumed α value. With the calculated specific attenuation, the total differential phase Φ_{DP} can be reconstructed with

$$\Phi_{DP, re} = \int_{r_0}^{r_m} \frac{2 \cdot A(s)}{\alpha} ds + \Phi_{DP}(r_0). \quad (9)$$

For a range of different α values, specific attenuation A and reconstructed Φ_{DP} is shown in Figure 6.

There is no single α value, for which the reconstructed Φ_{DP} matched the observed Φ_{DP} for all range gates. However, for each range gate, there is an optimal α value, which has the least difference between the reconstructed Φ_{DP} and the observed Φ_{DP} at that gate.

Differences between reconstructed and observed Φ_{DP} are shown in Figure 7, where a continuous line of low error exists. Clearly visible is the change of the α value along the radial associated with a transition from pure rain to primarily hail or rain/hail mixture.

For each range gate, the α value with the lowest error between reconstructed and observed Φ_{DP} can be selected. This gives the highest possible radial resolution for α , as for each range gate a different value is obtained.

For demonstration, these values have been used in combination with the Multi-Interval ZPHI-method as shown in Figure 8. The corrected reflectivity factor seems to be reasonable and the correction therefore valid. Of course, further testing and a validation of this method is required before it can be applied in operational service.

4. BACKSCATTERING SIMULATION

As a byproduct of the hail attenuation correction, difference in backscattering phase shift δ was estimated according to equation (8) and found to be varying between -30° and 30° throughout the June 2016 event. While these values seem reasonable and align with literature values, an assessment of theoretical possible δ values will be presented here.

4.1 Two-layer T-matrix backscattering simulation

A T-matrix simulation for two-layer spheroids is used to estimate backscattering characteristics of melting hail. The inner layer is consisting of solid ice, coated with a layer of water. Refractive indices are calculated based on equations from Cole-Cole (1941). The T-matrix code used is the same as in Ryzhkov *et al.* (2013a).

Our results are consistent with another two-layer T-matrix study of wet hail (Depue *et al.*, 2007). Figure 9 shows the result of our simulation, which mimics the computations of Depue *et al.* for “solid ice core with 0.5mm water coat and 25° canting angle” experiment of (see their Figure 2a, dashed line “W25”). Although the simulated differential reflectivity differs for higher diameters, the shape of the curve is quite similar. Since the exact refractive indices and temperature used in the study of Depue *et al.* (2007) are unknown, it is reasonable to assume that the difference in the curves might be due to an unknown difference in the refractive indices.

With the set of parameters shown in Table 1, the resulting polarimetric variables at C band simulated with the two-layer T-matrix code for wet hail are shown in Figure 10. Reflectivity factor, differential reflectivity, cross-correlation coefficient, and backscatter differential phase indicate a strong resonance for hail diameters of 19mm. A minor resonance is visible for 88mm. At resonance diameters, values of multiple simulated polarimetric variables reach both minima and maxima. δ completely wraps around for the major resonance diameter and reaches values from 25° to 55° otherwise.

Among all polarimetric variables, only specific attenuation A exhibits monotonic increase with hail diameter exceeding 15mm. This makes specific attenuation A a very promising parameter for hail size discrimination at C band. Other variables fluctuate between minima and maxima and their use for hail size discrimination might be therefore ambiguous.

4.2 Two-layer vs. single-layer

To test our version of two-layer T-matrix code, its performance was compared with the one of a traditional single-layer T-matrix method in dry hail. For the single-layer computations, code from Leinonen (2014) was used, which provides an easy-to-use Python implementation and is based on the code from Mishchenko *et al.* (1998). To have a comparable setup, both T-matrix simulations were made for dry hail. The results of the single-layer T-matrix simulation, the two-layer T-matrix simulation with double precision and the two-layer T-matrix simulation with quadruple precision are shown in Figure 11. The differences between these simulation results are minor, although, the two-layer T-matrix simulation shows less spurious fluctuations.

Melting hail without two-layer computation, could only be simulated by spongy ice in order to keep

the liquid water fraction the same. This is schematically shown in Figure 12.

CONCLUSIONS

We have demonstrated different approaches to correct attenuation caused by hail and discussed their benefits and flaws. The modified Hotspot/ZPHI-method has the highest reliability in terms of attenuation correction as it produced plausible α and attenuation corrected Z. The adaptive α scheme provides the highest radial resolution of α estimate. In combination with the multi-interval ZPHI-method, the adaptive α proved to yield reasonable attenuation corrected Z.

Detection and quantification of large hail can be problematic at C band. On the one hand, even small hail

can cause significant attenuation. On the other hand, due to backscattering resonance effects, the received signals may be ambiguous. However, the advanced hail attenuation correction scheme may address the problem (at least partially) and, moreover, can be used to quantify hail size and backscattering phase shift δ .

ACKNOWLEDGEMENTS

The polarimetric radar data and disdrometer data were kindly provided by the German Weather Service (DWD). This project is supported under grant 2015EMF-07.

TABLES

	Axis Ratio	Icecore Density	Thickness of water coat	Simulation Steps	Std.dev. canting angle	Temperature	Radar Wavelength
Wet Hail	0.75	0.93 g cm ⁻³	0.10 mm	0.10 mm	7.0°	0.0°C	C band

Table 1: Parameters for T-matrix hail simulation.

FIGURES

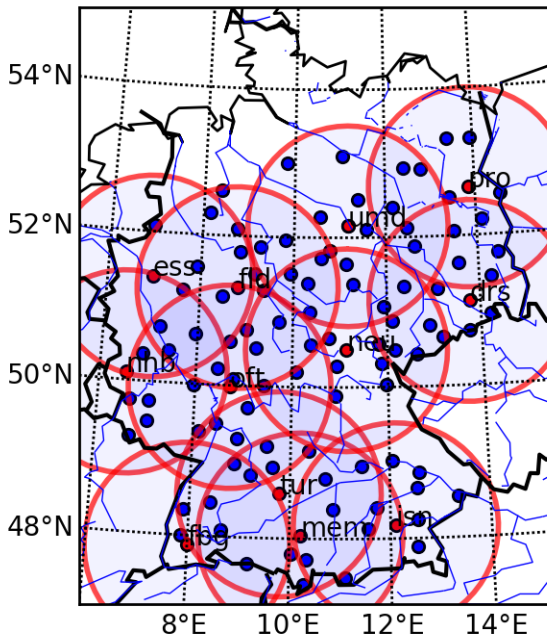


Figure 1: Location of C-band radar sites potentially available to be used in the study (marked as red dots; maximum ranges (180km) denoted by red rings) and disdrometer stations (marked as blue dots).

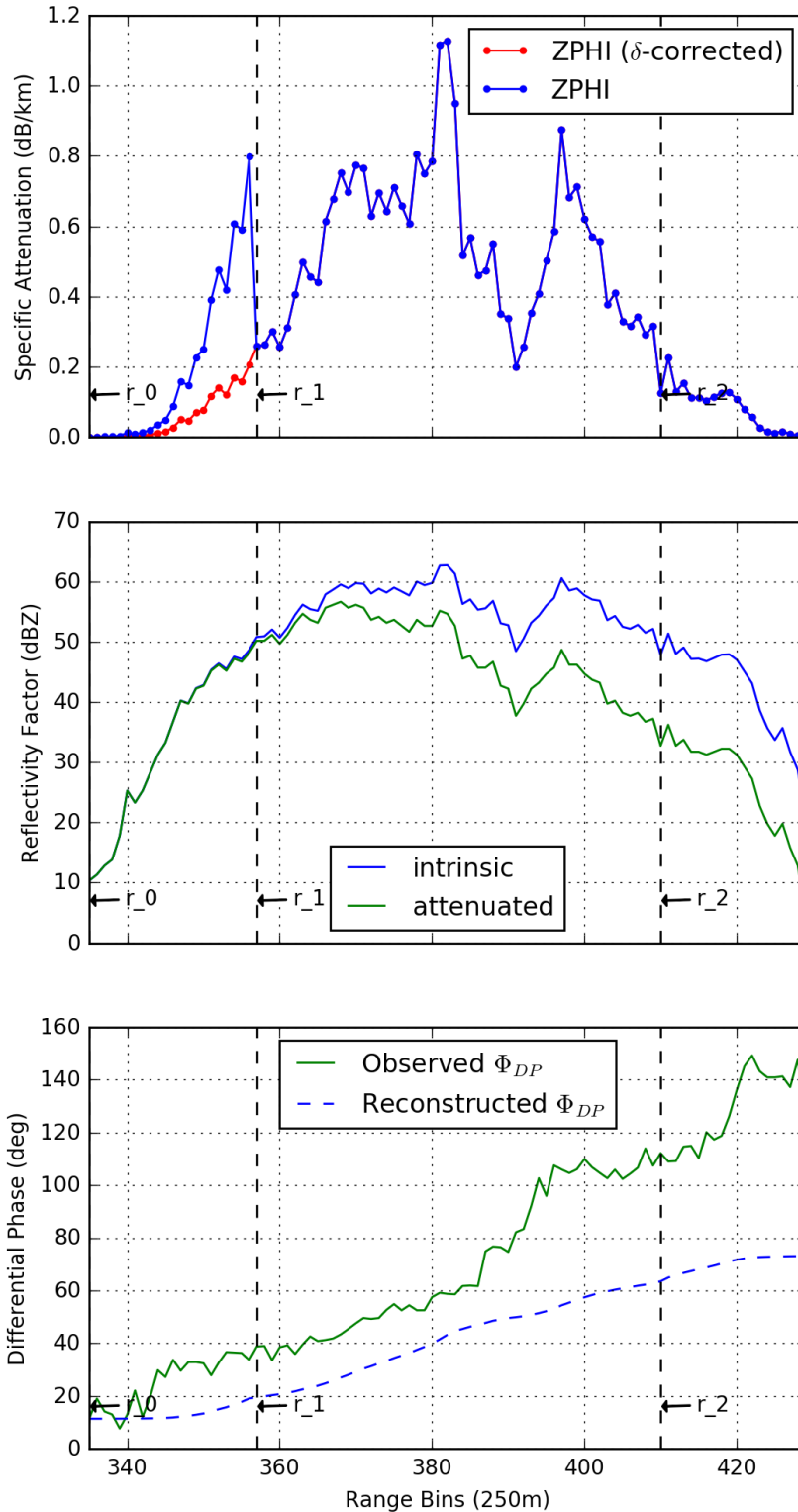


Figure 2: Calculated specific attenuation A , observed and corrected reflectivity factor Z and differential phase Φ_{DP} at 272° azimuth from C-band DWD radar 'Essen' at 2016-06-23, 18:50 UTC. The ray is segmented into intervals as written in the text. A is shown with neglecting δ (blue) and with considering δ (red).

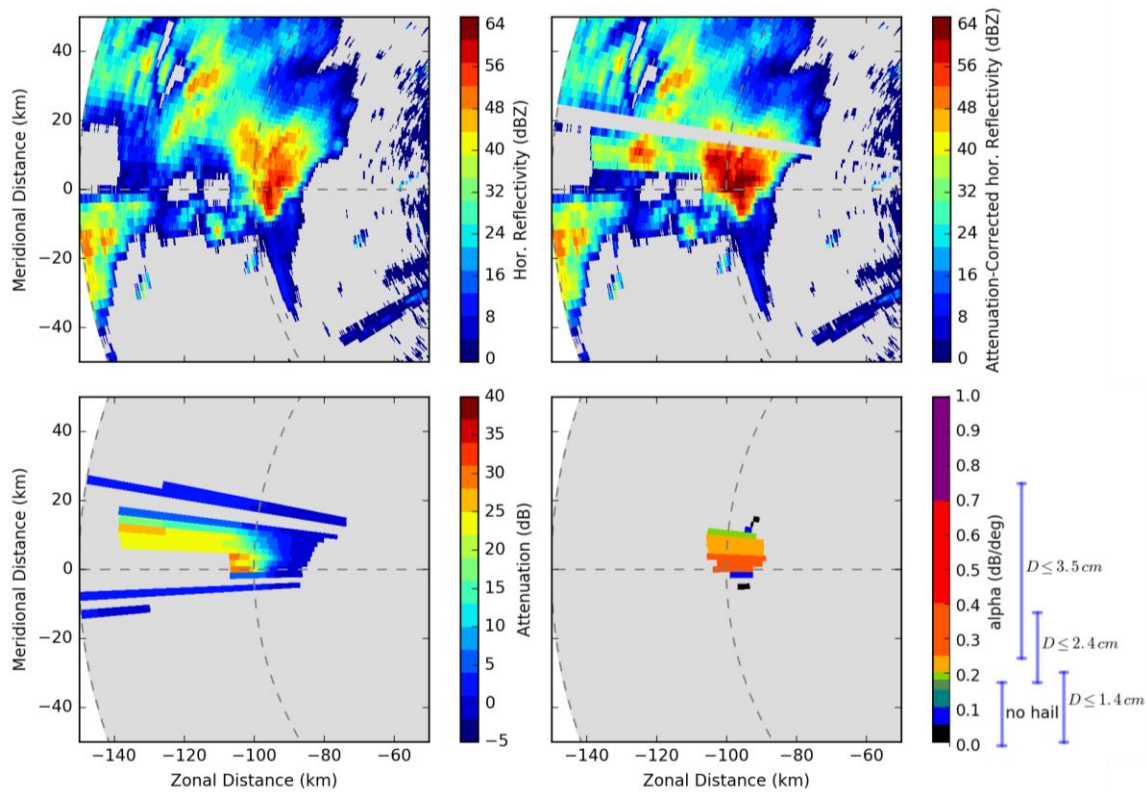


Figure 3: Observed and corrected reflectivity factor (upper row) and estimated attenuation by hail and α_{hail} (lower row), where ever applicable. Same radar, date and time as in Figure 2. Theoretical hail sizes for α ranges have been added to lower right panel for comparisons (adapted from Ryzhkov *et al.*, 2013b).

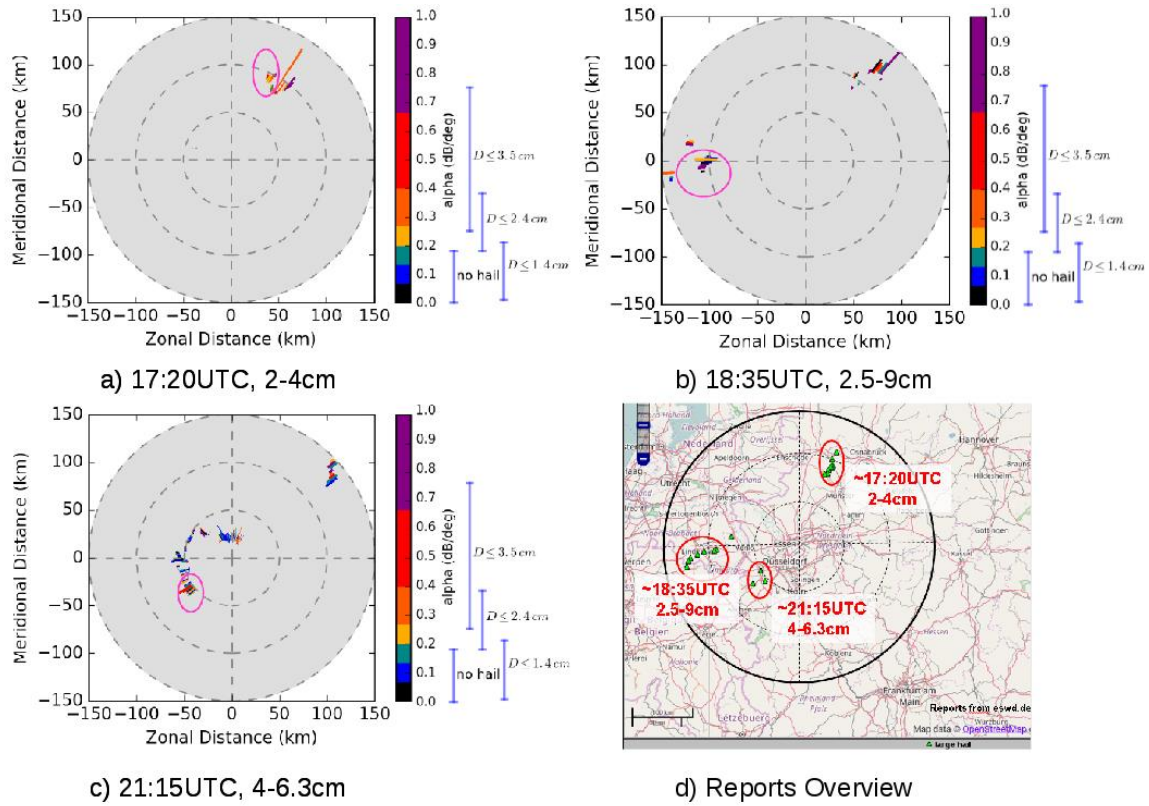


Figure 4: a),b),c): Estimated α for the same radar and event as in Figure 3, but for times were ground reports from ESWD indicated large hail. Locations of reports are shown circled in magenta. d) Reports for large hail from ESWD with ranges of maximum diameter between reports of similar area. Black ring shows maximum radar range of 180km.

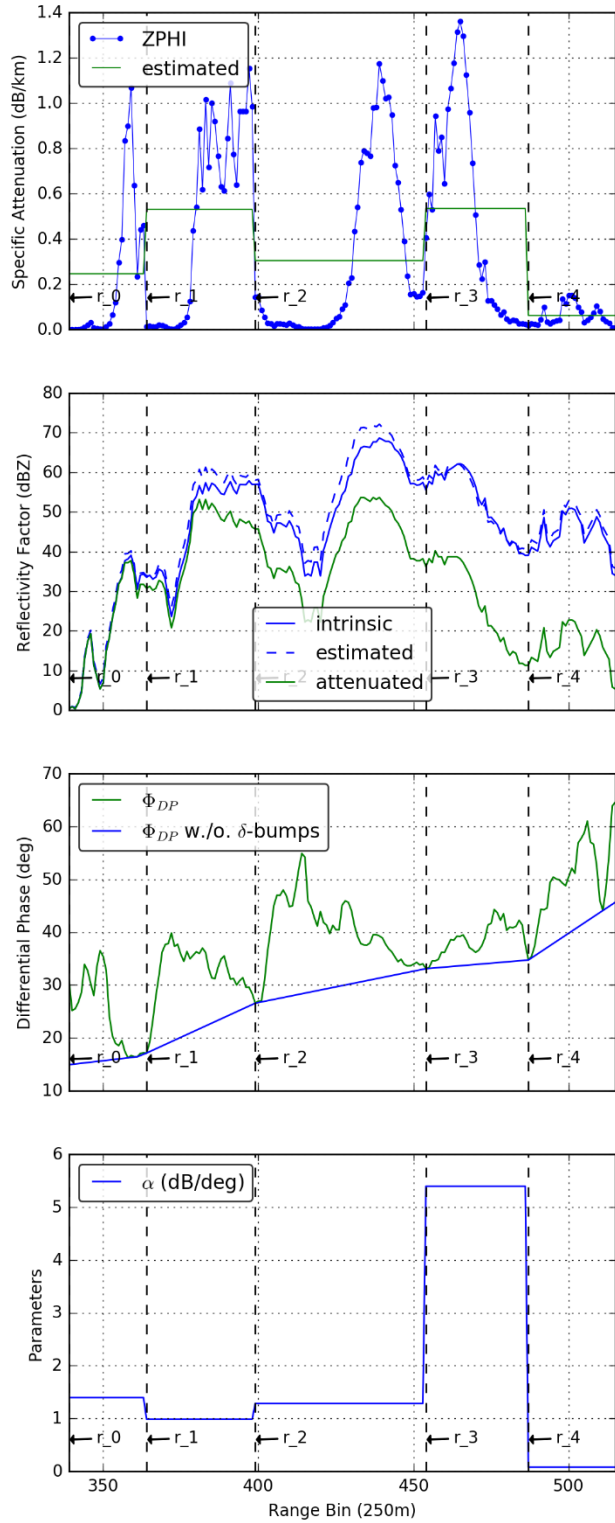


Figure 5: Similar to Figure 2, but calculations were done with the Multi-Interval ZPHI-method. Additionally, α is shown.

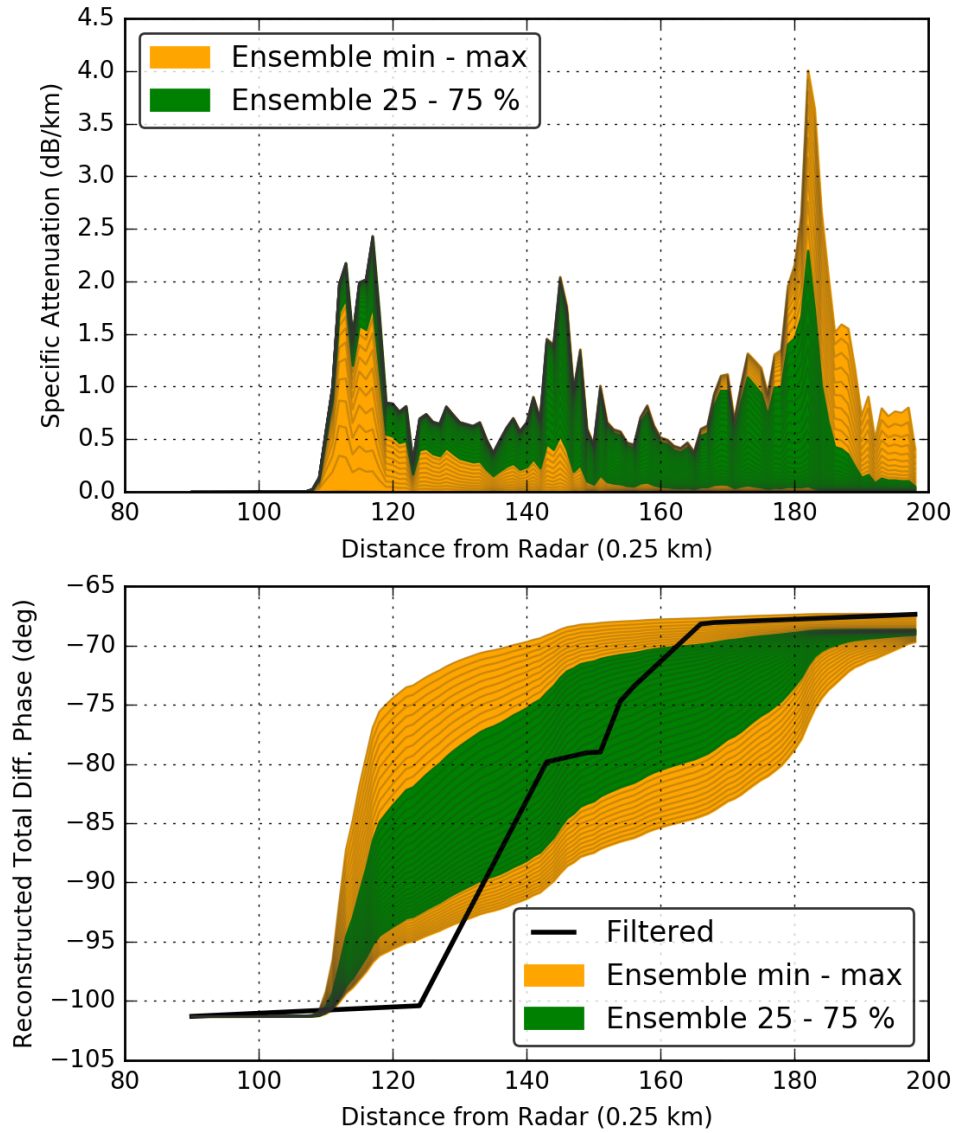


Figure 6: Possible value range for specific attenuation (upper plot) and reconstructed total differential phase (lower plot) for ZPHI-method with a range of α values. The filtered Φ_{DP} in the lower plot is the observed Φ_{DP} without “ δ -bumps” as shown in blue in Figure 5 (differential phase).

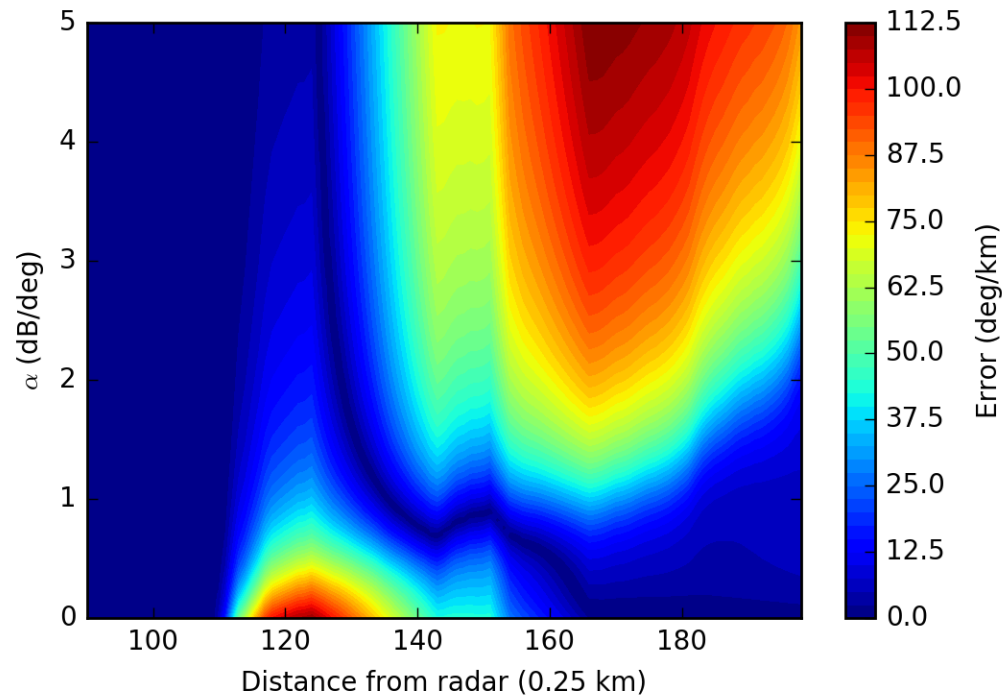


Figure 7: Absolute difference between observed Φ_{DP} and reconstructed Φ_{DP} (as in Figure 6) for each range gate and for each α value.

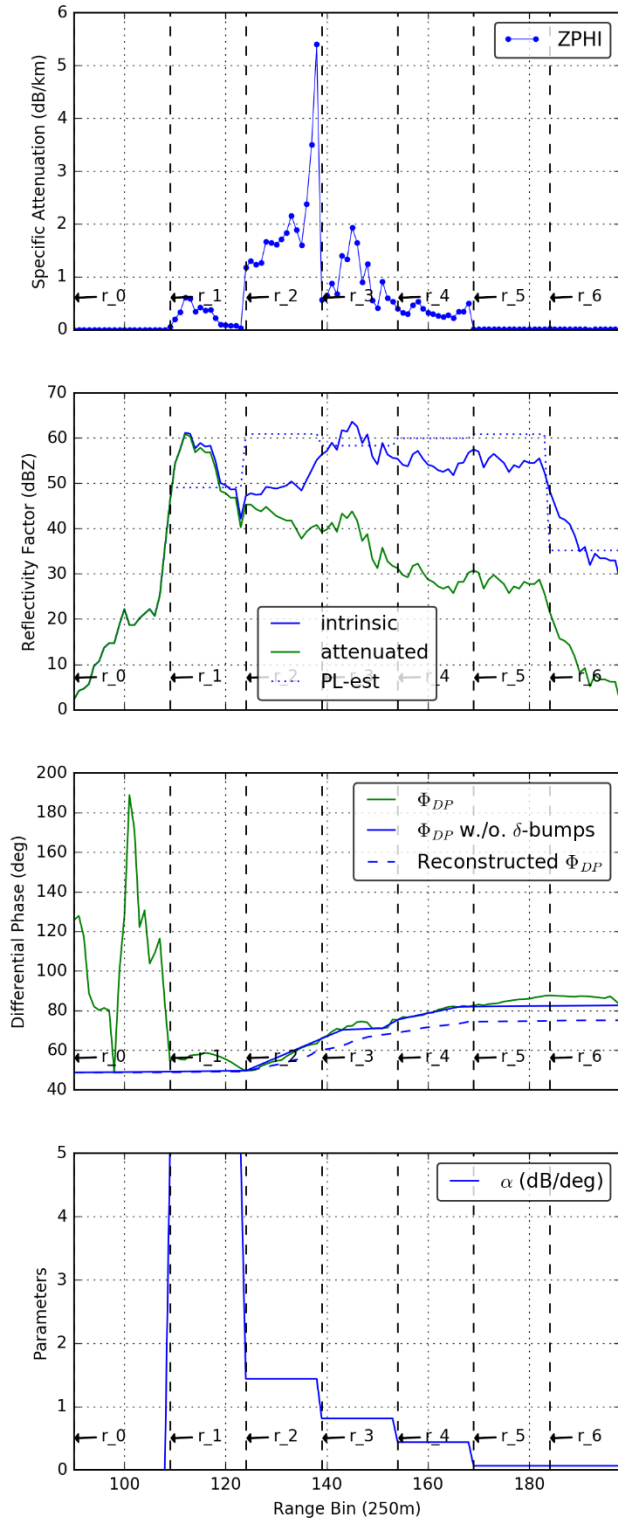


Figure 8: As in Figure 5, but with α from adaptive α scheme (as shown in Figure 7).

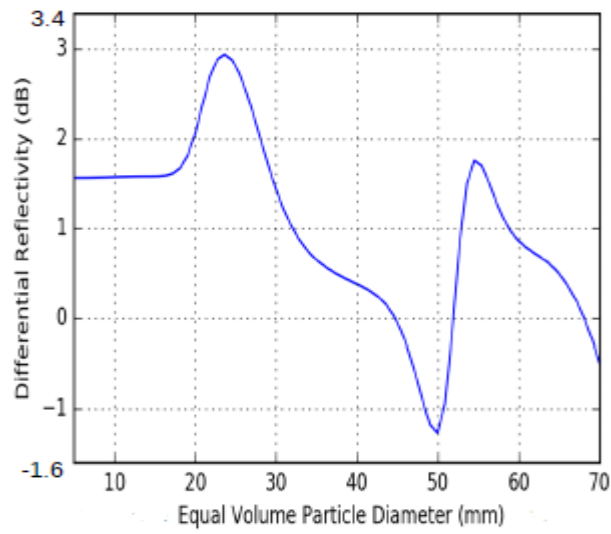


Figure 9: Simulated differential reflectivity as a function of equivolume particle diameter for wet hail. Two-layer T-matrix code from Ryzhkov *et al.* (2013a) was used.

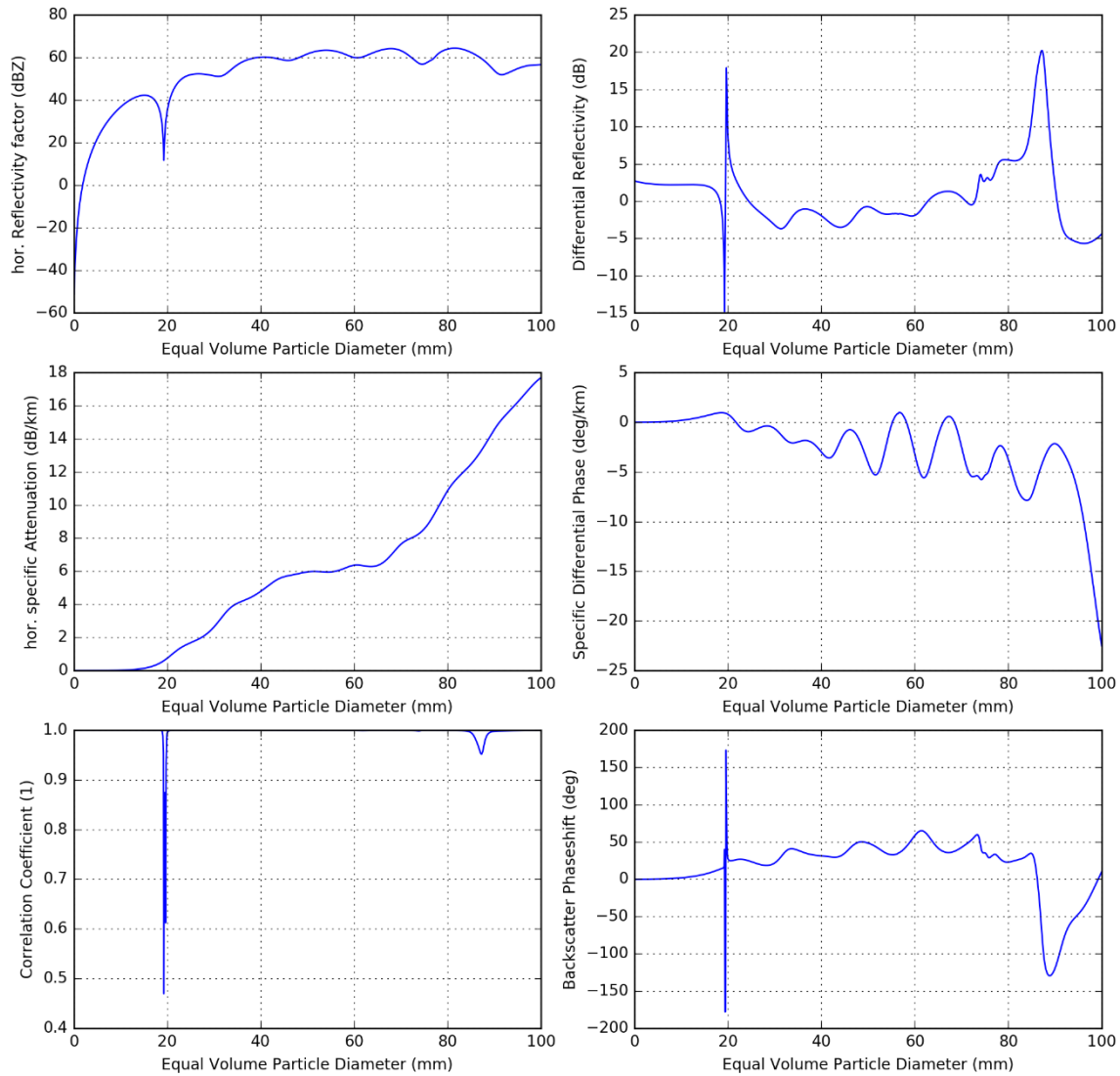


Figure 10: Simulated polarimetric variables for equivolume hail diameter. Two-layer T-matrix code from Ryzhkov *et al.* (2013a) was used. For details on the setup see Table 1.

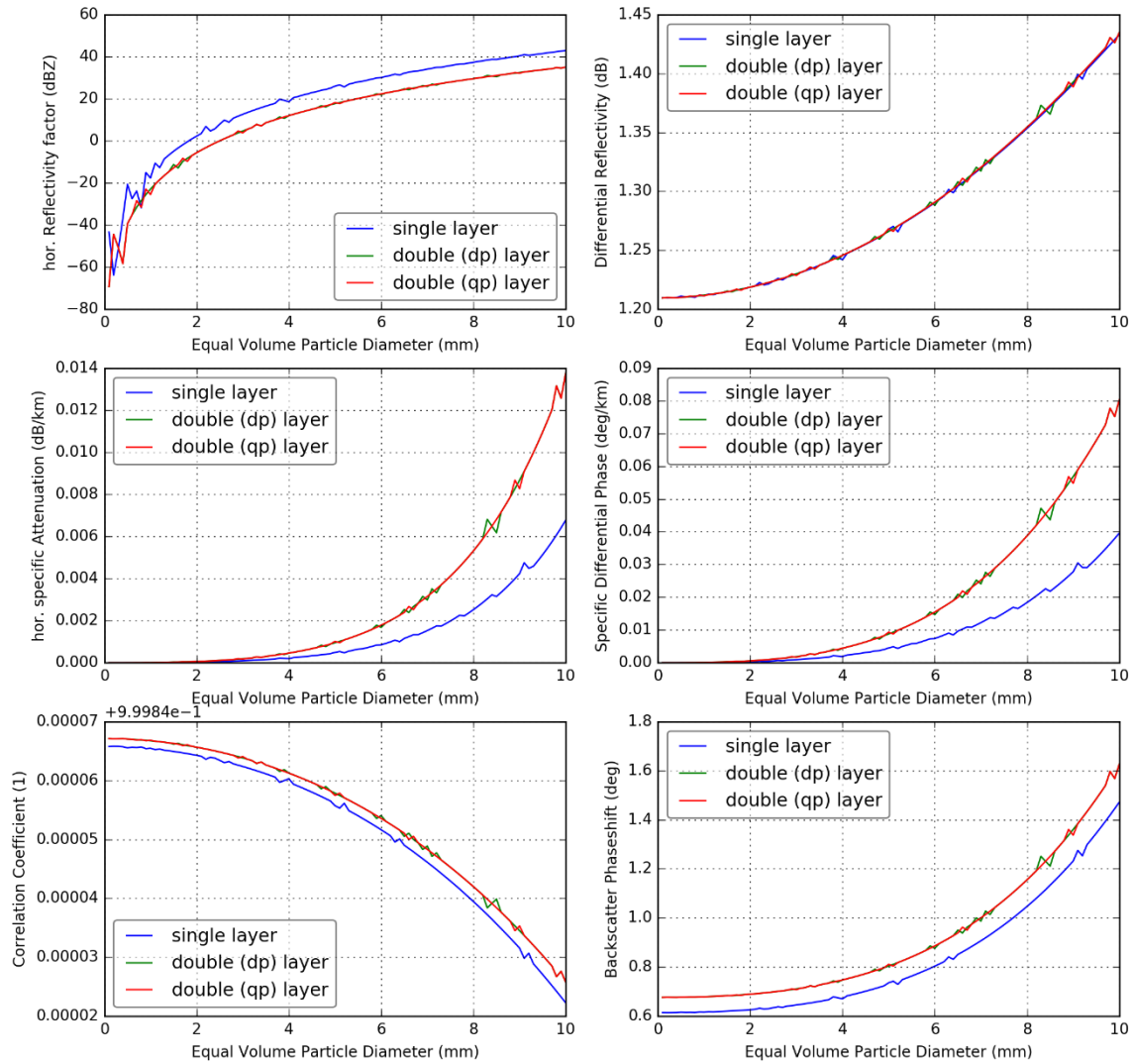


Figure 11: Same as in Figure 10, but for dry ice and with (in blue) single-layer T-matrix code from Leinonen (2014), (in green) two-layer T-matrix double precision as in Figure 10 and (in red) two-layer T-matrix code with quadruple precision.

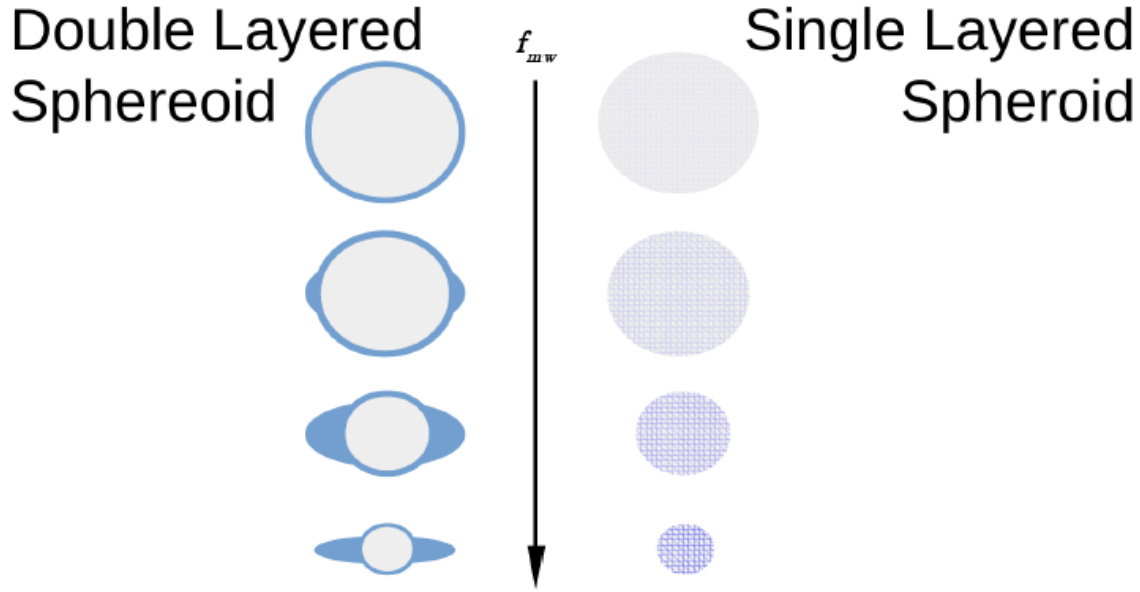


Figure 12: Schematic of wet hail and mass water fraction (f_{mw}) representation in two-layer and single-layer backscattering simulation models.

APPENDIX

The derivation to estimate δ with ZPHI-method is tedious but straight-forward. Defining the substitution

$$\exp(0.23b_h PIA(r_1, r_2)) - 1 = C(b_h, PIA(r_1, r_2)),$$

the deviation can be started with equation (1)

$$\Delta A_h(r_2) = A_h(r_2) - A_h(r_2 - 1) = A_h(r_2) - \frac{Z'(r_2 - 1)^{b_h} \cdot C(b_h, PIA(r_1, r_2))}{I(r_1, r_2) + C(b_h, PIA(r_1, r_2)) \cdot I(r_2 - 1, r_2)}$$

With the demand $\Delta A_h(r_2) \rightarrow 0$ and $A_h(r_2)$ being known the equation can be solved

$$\begin{aligned} \Rightarrow \Delta A_h(r_2) \rightarrow 0 &= A_h(r_2) - \frac{Z'(r_2 - 1)^{b_h} \cdot C(b_h, PIA(r_1, r_2))}{I(r_1, r_2) + C(b_h, PIA(r_1, r_2)) \cdot I(r_2 - 1, r_2)} \\ \Rightarrow Z'(r_2 - 1)^{b_h} \cdot C(b_h, PIA(r_1, r_2)) &= A_h(r_2) \cdot (I(r_1, r_2) + C(b_h, PIA(r_1, r_2)) \cdot I(r_2 - 1, r_2)) \\ \Rightarrow C(b_h, PIA(r_1, r_2)) \cdot (Z'(r_2 - 1)^{b_h} - A_h(r_2) \cdot I(r_2 - 1, r_2)) &= A_h(r_2) \cdot I(r_1, r_2) \end{aligned}$$

Using the substitution from above

$$\begin{aligned} \Rightarrow \exp(0.23b_h PIA(r_1, r_2)) - 1 &= A_h(r_2) \cdot \frac{I(r_1, r_2)}{Z'(r_2 - 1)^{b_h} - A_h(r_2) \cdot I(r_2 - 1, r_2)} \\ \Rightarrow \Phi_{DP}(r_2) - \Phi_{DP}(r_1) - (\delta(r_2) - \delta(r_1)) &= \frac{1}{0.23b_h \alpha_h} \ln \left[1 + A_h(r_2) \cdot \frac{I(r_1, r_2)}{Z'(r_2 - 1)^{b_h} - A_h(r_2) \cdot I(r_2 - 1, r_2)} \right] \\ \Rightarrow \delta(r_2) - \delta(r_1) &= \Phi_{DP}(r_2) - \Phi_{DP}(r_1) - \frac{1}{0.23b_h \alpha_h} \ln \left[1 + A_h(r_2) \cdot \frac{I(r_1, r_2)}{Z'(r_2 - 1)^{b_h} - A_h(r_2) \cdot I(r_2 - 1, r_2)} \right], \end{aligned}$$

which yields the desired equation.

REFERENCES

- Bringi, V. N., & Chandrasekar, V. (2001). *Polarimetric Doppler Weather Radar: Principles and Applications*. Cambridge University Press.
- Cole, K. S. (1941). Dispersion and absorption in dielectrics I. Alternating current characteristics. *The Journal of chemical physics*, 9(4), pp. 341-351.
- Depue, T. K., Kennedy, P. C., & Rutledge, S. A. (2007). Performance of the Hail Differential Reflectivity (H_DR) Polarimetric Radar Hail Indicator. *Journal of Applied Meteorology and Climatology*, 46(8), 1290-1301. Retrieved from <http://dx.doi.org/10.1175/JAM2529.1>

- Le Bouar, E., Testud, J., & Keenan, T. D. (2001). Validation of the Rain Profiling Algorithm "ZPHI" from the C-Band Polarimetric Weather Radar in Darwin. *Journal of Atmospheric and Oceanic Technology*, 18, 1819-1837.
- Leinonen, J. (2014). High-level interface to T-matrix scattering calculations: architecture, capabilities and limitations. *Optics Express*, 22(2), 1655-1660.
- Mishchenko, M. I. (1998). Capabilities and limitations of a current FORTRAN implementation of the T-matrix method for randomly oriented, rotationally symmetric scatterers. *Journal of Quantitative Spectroscopy and Radiative Transfer*, 60(3), 309-324.
- Ortega, K. L., Krause, J. M., & Ryzhkov, A. V. (2016). Polarimetric Radar Characteristics of Melting Hail. Part III: Validation of the Algorithm for Hail Size Discrimination. *J. Appl. Meteor. Climatol.*, 55(4), 829-848. Retrieved from <http://dx.doi.org/10.1175/JAMC-D-15-0203.1>
- Ryzhkov, A. V., Kumjian, M. R., Ganson, S. M., & Khain, A. P. (2013a). Polarimetric Radar Characteristics of Melting Hail. Part I: Theoretical Simulations Using Spectral Microphysical Modeling. *Journal of Applied Meteorology and Climatology*, 52(12), 2849-2870. Retrieved from <http://dx.doi.org/10.1175/JAMC-D-13-073.1>
- Ryzhkov, A. V., Kumjian, M. R., Ganson, S. M., & Zhang, P. (2013b). Polarimetric Radar Characteristics of Melting Hail. Part II: Practical Implications. *Journal of Applied Meteorology and Climatology*, 52(12), 2871-2886. Retrieved from <http://dx.doi.org/10.1175/JAMC-D-13-074.1>
- Testud, J., Le Bouar, E., Obligis, E., & Ali-Mehenni, M. (2000). The Rain Profiling Algorithm Applied to Polarimetric Weather Radar. *Journal of Atmospheric and Oceanic Technology*, 17(3), 332-356. Retrieved from [http://journals.ametsoc.org/doi/abs/10.1175/1520-0426\(2000\)017%3C0332:TRPAAT%3E2.0.CO;2](http://journals.ametsoc.org/doi/abs/10.1175/1520-0426(2000)017%3C0332:TRPAAT%3E2.0.CO;2)